NeuroImage: Clinical 9 (2015) 648–659

Contents lists available at ScienceDirect

NeuroImage: Clinical

journal homepage: www.elsevier.com/locate/ynicl

Abnormal white matter properties in adolescent girls with anorexia nervosa

Katherine E. Travis[a,*,1], Neville H. Golden[b,1], Heidi M. Feldman[a], Murray Solomon[c], Jenny Nguyen[b], Aviv Mezer[d], Jason D. Yeatman[e], Robert F. Dougherty[f]

[a] Division of Neonatal and Developmental Medicine, Department of Pediatrics, Stanford University School of Medicine, Palo Alto, CA 94303, USA
[b] Division of Adolescent Medicine, Department of Pediatrics, Stanford University School of Medicine, Palo Alto, CA 94303, USA
[c] Los Gatos MRI, Los Gatos, CA 95032, USA
[d] Edmond and Lily Safra Center for Brain Sciences (ELSC), The Hebrew University, Givat Ram, Jerusalem, 91904, Israel
[e] Institute for Learning & Brain Sciences and Department of Speech & Hearing Sciences, University of Washington, Seattle, WA, 98195, USA
[f] Stanford University Center for Cognitive and Neurobiological Imaging, Stanford, CA 94305, USA

ARTICLE INFO

Article history:
Received 17 August 2015
Received in revised form 13 October 2015
Accepted 15 October 2015
Available online 23 October 2015

Keywords:
Anorexia-nervosa
Adolescents
White matter
Diffusion
Quantitative MRI

ABSTRACT

Anorexia nervosa (AN) is a serious eating disorder that typically emerges during adolescence and occurs most frequently in females. To date, very few studies have investigated the possible impact of AN on white matter tissue properties during adolescence, when white matter is still developing. The present study evaluated white matter tissue properties in adolescent girls with AN using diffusion MRI with tractography and T1 relaxometry to measure R1 (1/T1), an index of myelin content. Fifteen adolescent girls with AN (mean age = 16.6 years ± 1.4) were compared to fifteen age-matched girls with normal weight and eating behaviors (mean age = 17.1 years ± 1.3). We identified and segmented 9 bilateral cerebral tracts (18) and 8 callosal fiber tracts in each participant's brain (26 total). Tract profiles were generated by computing measures for fractional anisotropy (FA) and R1 along the trajectory of each tract. Compared to controls, FA in the AN group was significantly decreased in 4 of 26 white matter tracts and significantly increased in 2 of 26 white matter tracts. R1 was significantly decreased in the AN group compared to controls in 11 of 26 white matter tracts. Reduced FA in combination with reduced R1 suggests that the observed white matter differences in AN are likely due to reductions in myelin content. For the majority of tracts, group differences in FA and R1 did not occur within the same tract. The present findings have important implications for understanding the neurobiological factors underlying white matter changes associated with AN and invite further investigations examining associations between white matter properties and specific physiological, cognitive, social, or emotional functions affected in AN.

1. Introduction

Anorexia nervosa (AN) is a serious eating disorder with high mortality (Arcelus et al., 2011). It is characterized by weight loss, cognitive distortions about shape and weight, and medical complications affecting almost every organ system (American Psychiatric Association, 2013). The onset of AN is typically in adolescence and the prevalence among girls is higher than the prevalence among boys (American Psychiatric Association, 2013). In recent years, the role of neurobiology of AN has become increasingly important for understanding the etiology and complications of the condition.

Structural brain changes have been identified in low weight patients with AN, and include reduced brain volume in both gray and white matter structures and enlarged lateral ventricles (Boghi et al., 2011; Castro-Fornieles et al., 2009; Golden et al., 1996; Hoffman et al., 1989; Katzman et al., 1996, 1997; Kingston et al., 1996; Muhlau et al., 2007; Roberto et al., 2011; Swayze et al., 1996, 2003). While the etiology of these changes has not yet been elucidated, decreased brain volumes observed in AN may, in part, reflect reductions in white matter volume that occur secondary to reductions in myelin content from the effects of malnutrition (Swayze et al., 2003). White matter, which is comprised of myelin-wrapped axons, continually develops throughout the second and third decades of life (Yakovlev and Lecours, 1967). Myelin is composed of various types of lipids and may therefore be particularly vulnerable to injury from malnutrition in AN during adolescence (Giedd, 2008). The impact of AN on white matter microstructure during adolescence has not been well characterized. We address this issue in the present study by exploring whether white matter tissue properties differ in a sample of adolescent girls with AN as compared to an age-matched sample of girls of normal weight and eating behaviors. To achieve this overall aim, we used two advanced structural neuroimaging techniques for assessing white matter microstructure: diffusion

* Corresponding author.
E-mail address: ktravis1@stanford.edu (K.E. Travis).
[1] These authors contributed equally and share the position of first author.

http://dx.doi.org/10.1016/j.nicl.2015.10.008

MRI (dMRI) analyzed with tractography and a novel quantitative magnetic resonance imaging (qMRI) method for measuring T1 relaxometry, R1 (1/T1), reflecting myelin content (Mezer et al., 2013).

Diffusion MRI is currently the most common structural neuroimaging method for assessing white matter changes associated with clinical conditions, such as AN. Diffusion MRI is most frequently analyzed using voxel-based or tractography approaches (Feldman et al., 2010). The predominate measure derived from dMRI to index white matter microstructure is fractional anisotropy (FA). FA serves as an index for the degree of water diffusion in a single direction in relation to diffusion in the perpendicular directions and is represented as a scalar value from 0 to 1 (Basser and Jones, 2002). In white matter regions in which fibers are coherently organized in a single direction, higher FA is typically associated with favorable neurobiological factors, such as increased myelination, greater axonal count, and higher axonal density (Basser and Pierpaoli, 1996; Beaulieu, 2002). However, in white matter regions of multiple fiber directions, FA in isolation is highly challenging to interpret (De Santis et al., 2014; Jeurissen et al., 2013; Jones and Cercignani, 2010).

Using voxel-based dMRI, several studies have observed decreased FA in adults with AN as compared to normal weight control adult subjects. Regions for decreased FA have been observed in distributed cortical white matter brain areas, including the bilateral fimbria-fornix, fronto-occipital fasciculus, posterior cingulate (Frank et al., 2013; Kazlouski et al., 2011), superior and posterior corona radiata (Frank et al., 2013; Frieling et al., 2012), optic radiations (Frieling et al., 2012), and the superior longitudinal fasciculus (Frieling et al., 2012; Via et al., 2014). However, not all studies of AN observe changes in FA (Yau et al., 2013). Failure to find group differences may be related to the biology of AN, such as stage of recovery following treatment (Yau et al., 2013), but may also reflect limitations in voxel-based methods for analyzing dMRI data (Jones and Cercignani, 2010), or difficulty detecting group FA differences with small sample sizes (De Santis et al., 2014). To our knowledge, only a single study has examined diffusion property changes associated with AN during adolescence (Frank et al., 2013). We require further studies of adolescents with AN to gain deeper understanding for whether changes in white matter properties during adulthood reflect persistent structural differences inherent to AN neuropathology beginning in adolescence, late alterations in tissue microstructure during adulthood, compensatory processes secondary to physiological manifestations of AN, or a combination of these possibilities. For this study, we chose to analyze dMRI data with tractography, an analytic approach that provides greater anatomical precision for identifying the specific white matter pathways and tract locations responsible for group differences than voxel-based approaches.

White matter tissue microstructure can also be examined using quantitative MRI approaches for measuring R1 (1/T1). R1 is a direct measure of the longitudinal relaxation rate of water protons in a magnetic field (Tofts, 2003). Rates of R1, measured in units of 1/s, are most affected by the amount of tissue contained within a voxel. Consequently, voxels comprised of mostly water typically have much slower R1 rates (~0.25/s) than voxels containing higher proportions of tissue (up to ~1.2/s). R1 rates are also sensitive to the biophysical characteristics of specific tissue types, particularly those affected by the presence of myelin (Bottomley et al., 1984; Kucharczyk et al., 1994; Mansfield, 1982; Rooney et al., 2007). In white matter, variations in myelin content account up to ~90% of R1 (Stuber et al., 2014), suggesting that R1 may be a useful proxy for tissue myeloarchitecture. R1 has also been shown to be directly related to tissue concentrations of iron (Stuber et al., 2014). Oligodendrocytes, the cells responsible for myelination within the central nervous system, are the predominant iron-containing cells of the brain (Connor and Menzies, 1996). Taken together, these features make R1 an important complement to diffusion measures, such as FA, which are indirect and open to multiple biological interpretations. Advances in qMRI methods now allow for the measurement of R1 with clinically-feasible scan times (Lutti et al., 2010; Mezer et al., 2013; Yarnykh, 2010). Techniques for mapping R1 have been combined with dMRI to assess changes in white matter tissue composition in relation neurological disorders known to affect myelin, such as multiple sclerosis (Mezer et al., 2013), and to dissociate among biological processes contributing to white matter changes observed during development and aging (Yeatman et al., 2014). To our knowledge, the present study is the first to employ both dMRI and R1 mapping techniques to evaluate white matter tissue properties in AN during adolescence. Using these two measures, we expected to gain further insight into white matter differences associated with AN that would not be distinguished with dMRI alone.

Based on the evidence described above, we hypothesized that, compared to controls, adolescent girls with AN would show evidence for decreased FA and decreased R1 in multiple white matter tracts. In particular, we expected to observe evidence for white matter property differences within pathways observed in previous dMRI studies to demonstrate differences in diffusion measures, including the fimbria-fornix, the inferior fronto-occipital, cingulate, and superior longitudinal fasciculus. Decreased FA in combination with decreased R1 would most likely reflect changes in white matter microstructure related to decreased myelin content. Findings from these analyses would contribute substantially to understanding neurobiological basis of white matter changes that have been previously observed in adult studies of AN. Documenting changes in white matter in girls with AN may prove important for understanding symptoms of the condition, including changes in physiological, cognitive, social, or emotional functions.

2. Materials and methods

2.1. Participants

Sixteen adolescent females between the ages of 14–18 years who met DSM-IV diagnostic criteria for AN (American Psychiatric Association, 2000), were recruited from the outpatient program of Lucile Packard Children's Hospital Stanford to participate in the study. At the time of MRI scanning, all AN participants were being treated medically as outpatients, were of low weight, but had stable vital signs. Inclusion criteria were low weight (<85% of expected body weight for age and height), endorsement of fear of gaining weight or becoming fat, body image distortion, and amenorrhea of greater than 3 months duration. Fifteen group age-matched controls were recruited from the community and from the Teen and Young Adult Clinic at Stanford to serve as controls. Inclusion criteria for controls were normal weight and no evidence of medical or psychiatric illness. Exclusion criteria included primary amenorrhea, and any contraindications to MRI scanning, such as metal heart valves, piercings, implants or jewelry that could not be removed. Based on these exclusion criteria, one AN subject with primary amenorrhea had to be excluded from the original AN group ($n = 16$) and the present analyses. Thus, the final number of participants analyzed for the AN group was 15 and for the control group 15. All AN subjects were of the restricting sub-type. Two AN subjects were on selective serotonin reuptake inhibitors, one on sertraline and one on fluoxetine. Subjects and controls were offered a monetary incentive for participation. This study was approved by the Institutional Review Board (IRB) at Stanford University. Written informed consent was obtained from each subject and a parent when the subject was a minor. Assent was obtained for those under the age of 18 years.

2.2. Clinical protocol

All study participants underwent a brief structured interview to confirm eligibility and to ensure subjects did not meet exclusion criteria. For those with AN, highest weight, lowest weight, current weight, rate of weight loss and duration of amenorrhea (in months) were recorded. The diagnosis of AN was confirmed by a board certified child psychiatrist. A neuroradiologist (MS) blind to the subjects' medical diagnosis, examined the high resolution T1-weighted scans collected as part of

the neuroimaging protocol and confirmed that none of the AN or control subjects demonstrated obvious structural abnormalities and ventricular size was determined to be within the normal range for all AN subjects. Both AN subjects and controls completed two self-administered validated questionnaires that quantify abnormal eating attitudes and behaviors, the Eating Attitudes Test (EAT-26) and the Eating Disorders Examination Questionnaire (EDE-Q). Questionnaire scoring was performed by one rater (JN) blind to the subjects' medical diagnosis. Height was measured in centimeters with patients barefoot using a wall-mounted stadiometer. Weight was measured to the nearest 0.1 kg on a single calibrated digital scale. Subjects were weighed post-voiding with the subjects undressed wearing only underwear and a hospital gown. Body mass index (BMI) was calculated (weight in kilograms divided by height in meters squared) and plotted on the Centers for Disease and Prevention growth charts. Percent median BMI was calculated as subject's BMI/median BMI for age and sex × 100.

2.3. dMRI acquisition and preprocessing

All MRI data were acquired on a 3 T GE Discovery MR750 scanner (General Electric Healthcare, Milwaukee, WI, USA) equipped with a 32-channel head coil (Nova Medical, Wilmington, MA, USA) at the Center for Cognitive and Neurobiological Imaging at Stanford University (www.cni.stanford.edu).

dMRI data were acquired with a diffusion-weighted, dual-spin-echo, echo-planar imaging (EPI) sequence with full brain coverage. Diffusion weighting gradients were applied at 96 non-collinear directions. In all subjects, dMRI data were acquired at 2.0 mm^3 spatial resolution and diffusion gradient strength was set to a b-value of 2500 s mm^{-2}. A set of 9 non-diffusion weighted b = 0 images were collected at the beginning of each scan.

Diffusion MR images were preprocessed with an open-source software, mrDiffusion (http://white.stanford.edu/newlm/index.php/MrDiffusion) implemented in MATLAB, R2013a (Mathworks, Natick, MA). The dual-spin echo sequence used here greatly reduces eddy-current distortions (Reese et al., 2003). For this reason, we did not need to perform eddy current correction. Subjects' motion in the diffusion weighted images was corrected using a rigid body alignment algorithm. Diffusion gradients were adjusted to account for the rotation applied to the measurements during motion correction (Rohde et al., 2004). A tensor model was fit to each voxel of the dMRI volume using a robust least-squares algorithm (RESTORE) that is designed to minimize the effects of pulsality and motion-related artifacts during the tensor fitting procedure (Chang et al., 2005). A continuous tensor field was estimated using trilinear interpolation of the tensor elements. We computed the eigenvalue decomposition of the diffusion tensor and the resulting eigenvectors were used to compute fractional anisotropy (FA; (Basser and Pierpaoli, 1996)).

2.4. Quantitative R1 mapping protocol

High-resolution T1-weighted anatomical images were collected for each subject using an 8-minute inversion recovery (IR)-prep 3D fast spoiled gradient (SPGR) sequence collected in the sagittal plane (0.8 mm cubed voxel size). This T1-weighted image was used as a common reference for alignment of the R1 and diffusion tensor image (DTI) maps.

We used a multiple-flip-angle procedure to estimate the R1 relaxation time (Fram et al., 1987). The flip angles measured were 4, 10, 20, and 30°, with 2 mm isotropic voxels, a TR of 14 ms and a TE of 3 ms. This resolution was chosen so that it would match the resolution of the diffusion images and so that it would be possible to acquire the four SPGR scans needed to estimate R1 in a time frame that was reasonable for a clinical sample. Since these methods are known to be biased due to RF transmit (B1) bias and inhomogeneity (Stikov et al., 2011), we corrected the bias by incorporating unbiased R1 values measured at lower resolution using a spin-echo inversion-recovery sequence with EPI read-out. Four inversion times were measured (2400, 1200, 400 and 50 ms), with 1.9 × 1.9 × 4 mm voxels, a TR of 3 s and a TE of 42 ms. The R1 fitting and bias correction used the same methods described in (Mezer et al., 2013).

2.5. Quantification of white matter tissue properties

The Automated Fiber Quantification (AFQ; https://github.jyeatman/AFQ) software package implemented in MATLAB was used to identify 18 cerebral white matter fiber tracts and 8 subdivisions of the corpus callosum in each participant's brain and quantify tract profiles of tissue properties along the tract trajectory (Yeatman et al., 2012, 2014).

AFQ uses a three-step procedure to identify each tract from an individual's dMRI data in native space. First, deterministic streamlines-tracking is used to estimate a whole-brain connectome of fiber tracts. Second, fiber tract segmentation is done based on the way-point region of interest (ROI) procedure and anatomical prescriptions as defined by (Wakana et al., 2004). In the way-point procedure, each fiber from the whole-brain connectome becomes a candidate for a specific fiber group if it passes through two ROIs that define the trajectory of the fiber group. Third, fiber tract refinement is done by comparing each candidate fiber to an established fiber tract probability map (Hua et al., 2008) and removing each candidate streamline that passes through regions of the white matter that are unlikely to be part of the tract. Steps two and three ensure that each fiber group passes through the two way-point ROIs that define the central trajectory of the pathway and also conform to the shape of the tracts as defined by fiber tract probability maps. Finally, the tract is summarized by a curve at the central position of all the tract fibers. The curve is created by defining 100 sample-points along each fiber and robustly computing the mean position of the corresponding sample points. The robust mean is computed by estimating the 3-dimensional Gaussian covariance of the sample points and removing fibers that are more than 5 standard deviations from the mean (Yeatman et al., 2012). Tissue properties are calculated along the trajectory of the fiber group by first resampling each fiber to 100 equally spaced nodes and then interpolating the value from a co-registered quantitative MRI image at each node along each fiber. The maps of scalar parameters from the dMRI data are already in register with the fiber tracts and do not require additional alignment.

To co-register a subject's quantitative R1 images to their dMRI data, we used the ANTS software package to warp the images to match the non-diffusion weighted, b0 image (Avants and Gee, 2004). This warping procedure corrects differences in image rotation and translation as well as local stretching and compression of the dMRI data due to EPI distortions. EPI distortions were minimal due to the 2× ASSET acceleration used for the readout of the diffusion-weighted images but some regions of the white matter were misaligned by 2–4 mm if a simple rigid body alignment was used. After applying the diffeomorphic warp, manual inspection of the aligned images confirmed that the registration was accurate within ~1 mm.

Tract profiles of each tissue parameter (FA and R1) were calculated as a weighted sum of each fiber's value at a given node where a fiber is weighted based on its Mahalanobis distance from the core of the tract. The result is a vector of 100 measurements of each diffusion and quantitative MRI parameter sampled equidistantly along the trajectory of each fascicle. Tract profiles can then be averaged to produce a single mean value for each tract or models can be fit at each point along the tract profile.

Using this procedure, we isolated for each individual 26 major pathways in the participant's native space. This included 8 pairs (16 total) of bilateral pathways that were segmented using the automated methods: anterior thalamic radiations (ATR), cingulum (Cing), corticospinal tract (CST), inferior fronto-occipital fasciculus (IFOF), inferior longitudinal fasciculus (ILF), anterior superior longitudinal fasciculus (aSLF), arcuate fasciculus (Arc) and the uncinate fasciculus (UF). One set of bilateral

tracts, the fimbria-fornix (F-F) was segmented manually (see subsequent section for this procedure). We also isolated 8 subdivisions of the corpus callosum using automated methods: orbitofrontal (Orb. Frontal); anterior frontal (Ant. Frontal); superior frontal (Sup. Frontal); motor, superior parietal (Sup. Parietal); posterior parietal (Post. Parietal), Temporal, and Occipital. In the present study, the corpus callosum refers to the entire collection of pathways observed to cross the mid-sagittal plane, including the midline structure. Fig. 1 shows the tracts, including the defining ROIs in a representative control participant.

2.6. Manual segmentation procedure: fimbria-fornix

Based on previous evidence demonstrating diffusion changes in the fimbria-fornix in adults with AN, we chose to manually segment both the left and right fimbria-fornix in participants. This was achieved by an expert (authors RFD and JN) manually selecting the fimbria-fornix fibers from whole-brain tractography fibers using the fiber visualization and selection tool Quench (Sherbondy et al., 2005). Although co-registration errors from EPI distortions were expected to be minimal in the present study (because diffusion data were acquired using an in-plane acceleration to shorten the read-out duration), the manual segmentation approach for the fimbria-fornix employed here ensured proper segmentation and helped to minimize potential errors from mis-alignment that have previously been shown for this pathway (Jones and Cercignani, 2010).

2.7. Statistical approach

2.7.1. Analyses of demographic and clinical variables

Two-tailed *t*-tests for independent samples were used to examine differences between the AN and control samples on demographic and clinical variables. Levene's test was used for equality of variance and the Mann Whitney U Test was used when significant difference in variance was detected. Data are presented as mean ± standard deviation (SD). Results were analyzed using SPSS v19.0 software (SPSS Inc, Chicago, IL).

2.7.2. Group comparisons of tract profiles

Two-tailed *t*-tests for independent samples were used to compare measures for FA and R1 from the AN and control group at each node along the tract profile of each tract. We employed a nonparametric permutation-based method to control for the comparisons performed along each tract and tract location ($100 \times 26 = 2600$; (Nichols and Holmes, 2001). This procedure produced a rigorous family-wise error corrected t-statistic and cluster size for each measure (FA or R1) that was corrected for between and along tract comparisons. Using this threshold, tract segments were considered to show significant group differences if differences occurred either (1) in a sufficient number of adjacent nodes to meet the criteria for a family-wise error corrected cluster size or (2) in nodes in which the effect size was greater than the critical t-value. We also considered group differences to be significant if (1) the effect size was greater than the critical t-value after controlling for along tract comparisons, or (2) if group differences occurred in a minimum of 10 adjacent nodes along FA or R1 tract profiles at $p < 0.05$, uncorrected. The degree of group differences was examined by comparing group mean FA or group R1 and the 95% confidence intervals computed for each tract segment found to demonstrate significant group differences. Follow-up analyses were next performed to confirm that between group differences were not due to age-related changes in either FA or R1 by performing one-way analysis of covariance ANCOVA for each tract found to demonstrate significant FA or R1 group differences. In these analyses, mean FA or mean R1 from significant tract locations served as the between subjects variable and age served as the covariate.

2.7.3. Secondary analyses: associations with clinical variables

To further interrogate group differences, we performed associative analyses to examine whether white matter measures (FA or R1) would be related to individual variations in measures for clinical severity, as indexed by body mass index (BMI), and percent median BMI, and individual variations in psychological characteristics of AN, including cognitive attitudes towards eating, body size and weight as measured by the EDE-Q composite measure. Specifically, we calculated Spearman rank correlations between each clinical variable and mean FA or mean R1 computed from tract segments demonstrating significant group differences after correction for multiple comparisons. This analysis was limited to the AN group to avoid a pseudo-correlation reflecting the group differences in both variables. Spearman rank correlations were used due to evidence for non-normal distribution in tract FA and R1 measures in preliminary exploration of the data. Associations were considered significant at $p < 0.05$.

3. Results

3.1. Demographic and clinical variables

Table 1 shows that AN subjects and controls were similar in age. Compared to controls, those with AN had a significantly lower

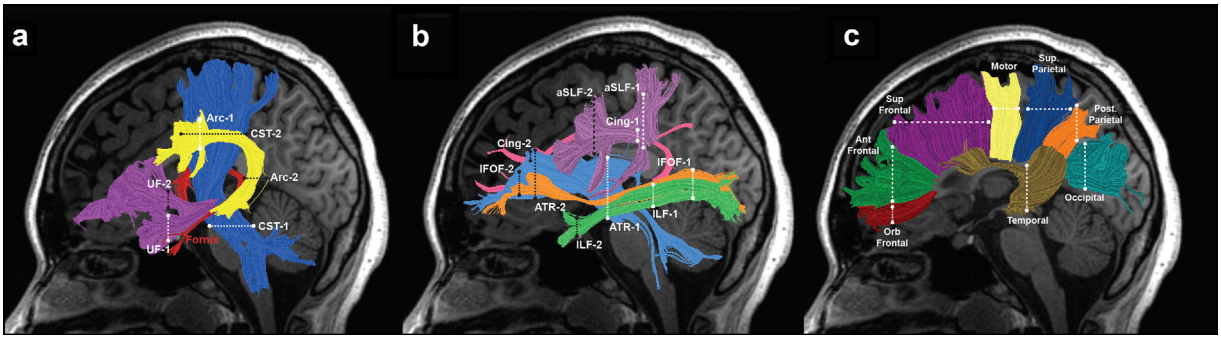

Fig. 1. Tractography of 26 major cerebral and callosal white matter tracts. Left hemisphere cerebral tracts are displayed on mid-sagittal T1 images from a representative control subject (a–c). Right hemisphere tract renderings not shown. Panel a illustrates the following cerebral white matter tracts: arcuate fasciculus (Arc) = yellow; corticospinal tract (CST) = blue; uncinate fasciculus (UF) = purple; fimbria-fornix (F-F) = red. Panel b illustrates the following cerebral white matter tracts: anterior thalamic radiation (ATR) = light blue; cingulum (Cing) = pink; inferior fronto-occipital fasciculus (IFOF) = orange; inferior longitudinal fasciculus (ILF) = green; anterior superior longitudinal fasciculus (aSLF) = lavender. Panel c illustrates 8 subdivisions of the corpus callosum: orbitofrontal (Orb Frontal) = dark red; anterior frontal (Ant. Frontal) = green; superior frontal (Sup. Frontal) = purple; motor = yellow; superior parietal (Sup. Parietal) = blue; posterior (Post. Parietal) = orange; temporal = brown; occipital = teal. Dashed lines represent the location of the regions of interest (ROIs) used to isolate each cerebral tract; ROI 1, white; ROI 2, black. ROIs are not indicated for F-F (red lettering) as this tract was segmented manually.

Table 1
Demographic and clinical variables: anorexia nervosa versus healthy controls.

	Anorexia nervosa N = 15		Controls N = 15		p
	Mean ± SD	Range	Mean ± SD	Range	
Age, years	16.6 ± 1.4	14.3–18.8	17.1 ± 1.3	14.5–18.9	.39
Weight, kg	43.7 ± 5.2	34.3–52.3	57.1 ± 9.0	43.4–76.6	<.001*
BMI, kg/m^2	16.0 ± 1.2	13.9–18.3	21.4 ± 2.1	18.6–24.7	<.001*
% median BMI	77.4 ± 4.9	0.0–9.0	102.8 ± 10.1	15.0–84.0	<.001*
Lifetime lowest BMI, kg/m^2	15.2 ± 1.2	13.6–17.2	n/a	n/a	n/a
Illness duration, months	16.3 ± 11.4	3–36	n/a	n/a	n/a
EAT-26	41.2 ± 16.3	9–60	3.1 ± 4.2	0–17	<.001*
EDE-Q total	3.4 ± 1.5	0.8–5.1	.47 ± .47	0.03–1.3	<.001*
EDE-Q restraint	3.3 ± 1.7	0–5.4	.36 ± .46	0–1.8	<.001*
EDE-Q eating control	3.0 ± 1.3	0.4–4.6	.20 ± .35	0–1.2	<.001*
EDE-Q shape concerns	3.9 ± 2.1	0.8–5.9	.73 ± .65	0.5–2.1	<.001*
EDE-Q weight concerns	3.4 ± 1.7	0.6–5.8	.59 ± .65	0–2.2	<.001*

SD = standard deviation; kg = kilograms; m = meters.
* Significant at $p < 0.005$, corrected.

mean weight ($p < .001$), BMI ($p < .001$), lower percent median BMI ($p < .001$) and higher scores on all measures of eating disorder symptomatology ($p < .001$).

3.2. Fiber tracking

Using whole-brain tractography, we segmented 9 bilateral cerebral white matter tracts and 8 subdivisions of the corpus callosum in both AN and control individuals (Fig. 1). In one AN and one control subject, we were unable to reliably identify the orbitofrontal subdivision of the corpus callosum. Visual inspection confirmed that ROIs used to segment the orbitofrontal subdivision were accurately placed. The results for the remaining participants are included in the analyses. In addition, we were unable to identify the Arc-R in 2 AN subjects. We attribute the difficultly in identifying the Arc-R to limitations of deterministic tractography approaches that cannot account for higher tract curvature and increased partial voluming with the aSLF-R, a finding consistent with several other reports (Catani et al., 2007; Lebel and Beaulieu, 2009; Mishra et al., 2010; Yeatman et al., 2011).

3.3. Group comparisons

Mean Tract FA and R1 profiles from the AN and control groups for all fiber tracts are presented in Figs. 2 and 3. Tracts are separated into two figures for visualization purposes. Tract FA and R1 profiles presented in Fig. 2 correspond to cerebral tracts shown in Fig. 1a,b. Tract FA and R1 profiles presented in Fig. 3 correspond to subdivisions of the corpus callosum shown in Fig. 1c. Results of group comparisons are described based on the order that tracts appear in Figs. 2 and 3. Tables 2 and 3 reflect the results of statistical comparisons performed to examine group differences in cerebral tracts and subdivisions of the corpus callosum, respectively.

3.4. Tract FA profiles

Analyses of tract FA profiles revealed that the AN group demonstrated both significantly decreased and increased FA as compared to the control group in 6 of 18 cerebral tracts (Fig. 2a1–a18) and 1 of 8 subdivisions of the corpus callosum (Fig. 3b1–b8) examined. In cerebral white matter tracts (Table 2), the AN group demonstrated significantly decreased FA ($p < 0.05$, uncorrected) within segments of the aSLF-R (Fig. 2a12), and F-F bilaterally (Fig. 2a17–a18). In contrast, the AN group demonstrated significantly increased FA ($p < 0.05$, corrected) within segments of the ATR-R (Fig. 2a2) and aSLF-L (Fig. 2a11). Within the corpus callosum (Table 3), the AN group demonstrated significantly decreased FA ($p < 0.05$, corrected) in the motor subdivision (Fig. 3a4). No other subdivisions of the corpus callosum were observed to demonstrate significant group FA differences. ANCOVA analyses confirmed that group FA differences remained significant ($p < 0.05$) for all tracts after controlling for age.

3.5. Tract R1 profiles

Analyses of tract R1 profiles revealed that the AN group demonstrated significantly decreased R1 in 6 of 18 cerebral tracts (Fig. 2b1–b18) and 5 of 8 subdivisions of the corpus callosum (Fig. 3b1–b8) examined. In cerebral white matter tracts (Table 2), the AN group demonstrated significantly decreased R1 ($p < 0.05$, corrected) as compared to the control group in a major segment of the CST-L (Fig. 2b5). The AN group demonstrated significantly decreased R1 ($p < 0.05$, corrected) in the Cing-L (Fig. 2b3), CST-R (Fig. 2b6), IFOF-L (Fig. 2b7), and bilateral Arc (Fig. 2b13–b14). Within the corpus callosum (Table 3), the AN group demonstrated significantly decreased R1 ($p < 0.05$, corrected) as compared to the control group within a large segment of the motor subdivision of the corpus callosum (Fig. 3b4). The AN group also demonstrated significantly decreased R1 ($p < 0.05$, corrected) as compared to the control group in the following subdivisions of the corpus callosum: Ant. Frontal, Sup. Parietal, Temporal, and Occipital (Fig. 3b2,b5,b7,b8, respectively). ANCOVA analyses confirmed that group R1 differences remained significant for all tracts after controlling for age except for the right and left arcuate in which group differences demonstrated trends towards significant group differences: $p = 0.073$ and $p = 0.079$, respectively.

3.6. Secondary analyses: associations with clinical variables

We performed secondary analyses to examine to whether group differences in white matter microstructure would be explained by individual variations in BMI and psychological attitudes and behaviors related to eating in the AN group. These analyses revealed no evidence for any significant associations ($p < 0.05$) between either of the white matter measures (FA or R1) and clinical measures for BMI and a composite measure from the EDE-Q.

4. Discussion

4.1. Summary of findings

In this study of adolescent girls with AN and age-matched controls with normal weight and normal eating behavior, we analyzed white

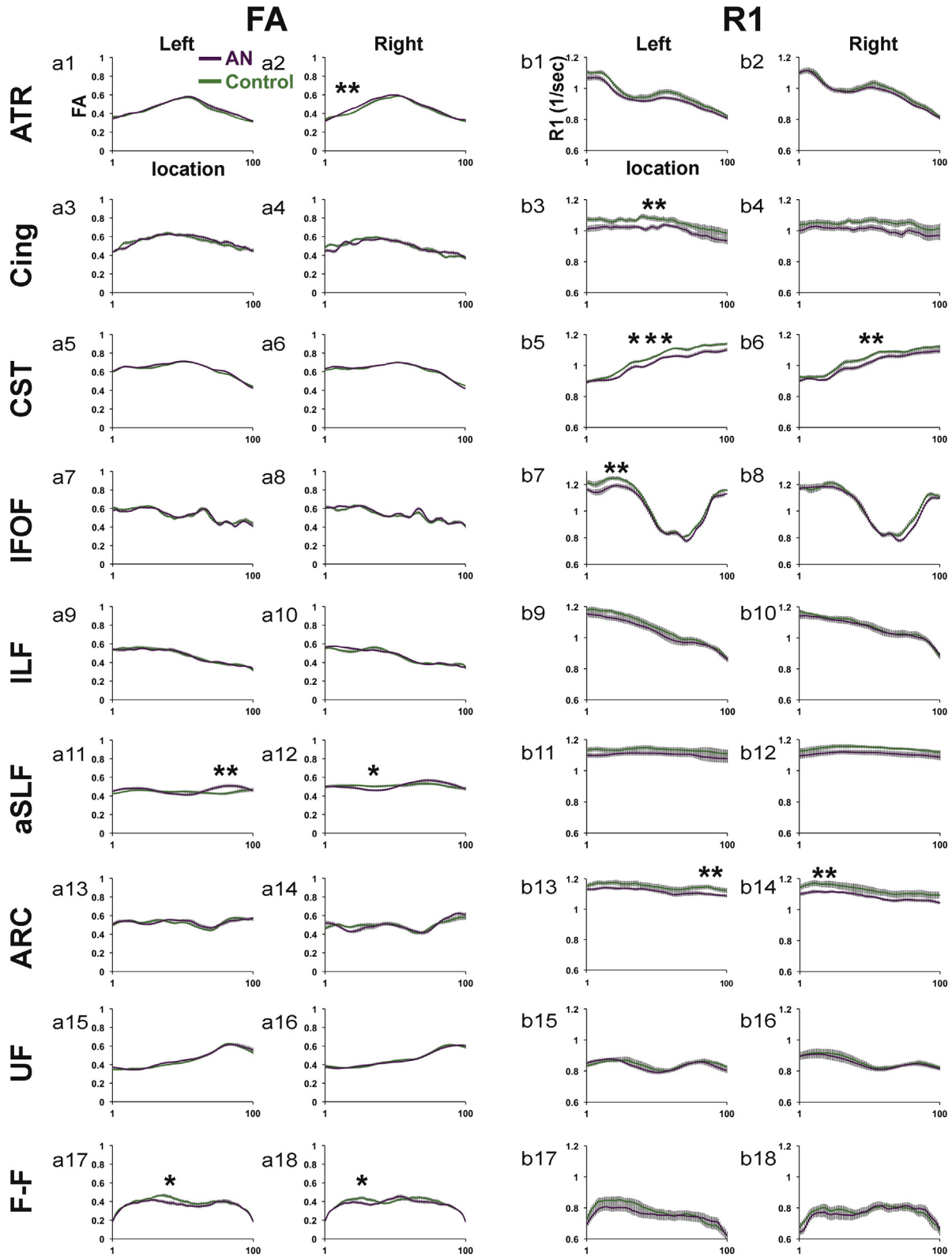

Fig. 2. FA and R1 tract profiles for the AN and control group for 18 cerebral white matter pathways. Mean FA (a1–a18) and Mean R1 (b1–b18) tract profiles are shown for each of the cerebral tracts depicted in Fig. 1a,b for the AN group (solid purple line) and the control group (solid green line). Group Mean FA and Mean R1 values are plotted for 100 equidistant nodes between the two ROIs used to isolate the core of each tract. Vertical bars along FA and R1 tract profiles indicate ± 1 standard error of the mean. Tracts demonstrating significant group differences ($p < 0.05$, uncorrected) are indicated with a single *. Tracts demonstrating group differences that were significant ($p < 0.05$) after correcting for along tract comparisons are indicated with two **. Tracts demonstrating group differences that were significant ($p < 0.05$) after correcting for between and along tract comparisons are indicated with three ***. ATR = anterior thalamic radiations; Cing = cingulate; CST = corticospinal tract; IFOF = inferior fronto-occipital fasciculus; ILF = inferior longitudinal fasciculus; aSLF = anterior superior longitudinal fasciculus; ARC = arcuate fasciculus; UF = uncinate fasciculus; F-F = fimbria-fornix; L = left; R = right.

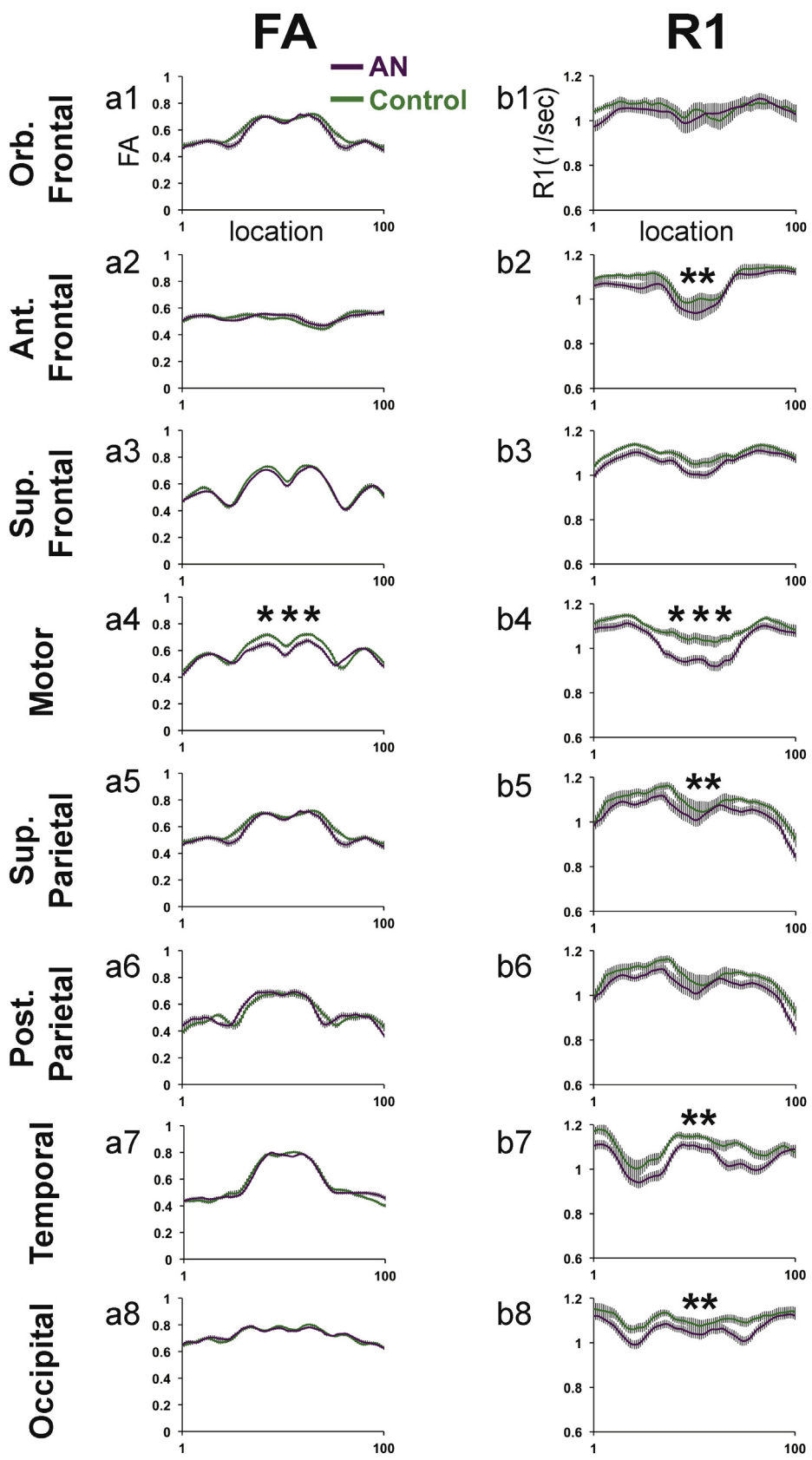

Fig. 3. FA and R1 tract profiles for the AN and control group for 8 subdivisions of the corpus callosum. Mean FA (a1–a8) and Mean R1 (b1–b8) tract profiles are shown for each of the cerebral tracts depicted in Fig. 1c for the AN group (solid purple line) and the control group (solid green line). Group Mean FA and Mean R1 values are plotted for 100 equidistant nodes between the two ROIs used to isolate the core of each tract. Vertical bars along FA and R1 tract profiles indicate ± 1 standard error of the mean. Tracts demonstrating group differences that were significant ($p < 0.05$) after correcting for along tract comparisons are indicated with two **. Tracts demonstrating group differences that were significant ($p < 0.05$) after correcting for between and along tract comparisons are indicated with three ***. Ant = anterior; Orb = orbital; Sup = superior; Post = posterior.

Table 2
Comparison of group mean FA or group mean R1 computed from tract segment (location) demonstrating significant group differences for bilateral cerebral white matter tracts.

Cerebral white matter tract	FA			R1		
	Location	AN Mean of cluster (95% CI)	Control Mean of cluster (95% CI)	location	AN Mean of cluster (95% CI)	Control Mean of cluster (95% CI)
ATR						
Left	–	–	–	–	–	–
Right	14–27**	0.45 (0.44–0.47)	0.41 (0.40–0.43)	–	–	–
Cing						
Left	–	–	–	30–53**	1.01 (0.97–1.05)	1.08 (1.05–1.11)
Right	–	–	–	–	–	–
CST						
Left	–	–	–	31–100***	1.04 (1.01–1.07)	1.09 (1.08–1.11)
Right	–	–	–	33–63**	0.99 (0.96–1.02)	1.04 (1.02–1.06)
IFOF						
Left	–	–	–	11–30**	1.16 (1.12–1.21)	1.24 (1.21–1.27)
Right	–	–	–	–	–	–
ILF						
Left	–	–	–	–	–	–
Right	–	–	–	–	–	–
aSLF						
Left	71–89**	0.50 (0.46–0.54)	0.43 (0.40–0.46)	–	–	–
Right	26–46*	0.47 (0.44–0.49)	0.50 (0.48–0.53)	–	–	–
Arc						
Left	–	–	–	82–94**	1.11 (1.07–1.16)	1.15 (1.13–1.18)
Right	–	–	–	4–21**	1.11 (1.07–1.15)	1.16 (1.14–1.19)
UF						
Left	–	–	–	–	–	–
Right	–	–	–	–	–	–
F-F						
Left	32–43*	0.40 (0.36–0.43)	0.46 (0.43–0.49)	–	–	–
Right	25–35*	0.38 (0.34–0.41)	0.43 (0.39–0.46)	–	–	–

CI = confidence interval; ATR = anterior thalamic radiations; Cing = cingulate; CST = corticospinal tract; IFOF = inferior fronto-occipital fasciculus; ILF = inferior longitudinal fasciculus; aSLF = anterior superior longitudinal fasciculus; ARC = arcuate fasciculus; UF = uncinate fasciculus; F-F = fimbria-fornix.
* Significant ($p < 0.05$, uncorrected).
** Significant ($p < 0.05$, corrected for along tract comparisons).
*** Significant ($p < 0.05$, corrected for between and along tract comparisons).

matter microstructure using two complementary methods for assessing white matter tissue properties: dMRI analyzed with tractography and quantitative MRI methods for mapping R1. We examined a total of 26 cerebral and callosal white matter tracts, thereby evaluating most of the major white matter pathways. We hypothesized that compared to controls, adolescent girls with AN would show decreased FA and decreased R1, suggestive of reduced myelin content, in one or more tracts. We generally confirmed the hypotheses. Compared to controls, FA in the AN group was significantly lower in 4 of 26 tracts, though FA was higher in 2 tracts, and R1 was significantly decreased in the AN group in 11 of the 26 white matter tracts examined. Group FA and group R1 differences remained significant after controlling for age in the majority of tracts. The present findings demonstrate that disturbances in white matter tracts are present in AN during adolescence and that these changes are likely to reflect alterations in myelin content.

4.2. Group differences in FA

Consistent with our initial predictions, measures for FA were found to be significantly decreased in the AN as compared to the control group within cerebral white matter tracts previously found to have decreased FA during adulthood and adolescence (Frank et al., 2013; Frieling et al., 2012; Kazlouski et al., 2011), including bilateral segments of the fimbria-fornix and the right aSLF. Evidence for decreased FA in adolescents with AN suggests that structural differences within these pathways are already present after a relatively short duration of illness. Longitudinal studies of individuals diagnosed with AN should explore whether structural differences in these pathways vary in association with disorder severity, illness duration, and whether such differences resolve after weight restoration following treatment. Such studies will be important for

Table 3
Comparison of group mean FA or group mean R1 computed from tract segment (location) demonstrating significant group differences for subdivisions of the corpus callosum.

Callosal subdivisions	FA			R1		
	Location	AN Mean of cluster (95% CI)	Control Mean of cluster (95% CI)	Location	Control Mean of cluster (95% CI)	AN Mean of cluster (95% CI)
Orb. Frontal	–	–	–	–	–	–
Ant. Frontal	–	–	–	10–24**	1.04 (1.00–1.09)	1.11 (1.09–1.13)
Sup. Frontal	–	–	–	–	–	–
Motor	29–75***	0.61 (0.58–0.65)	0.67 (0.64–0.70)	31–72***	0.95 (0.90–1.00)	1.05 (1.02–1.09)
Post. Parietal	–	–	–	–	–	–
Sup. Parietal	–	–	–	59–76**	1.03 (0.98–1.09)	1.11 (1.08–1.14)
Occipital	–	–	–	67–81**	1.02 (0.97–1.07)	1.10 (1.07–1.14)
Temporal	–	–	–	64–83**	1.00 (0.95–1.06)	1.10 (1.06–1.13)

CI = confidence interval; Ant = anterior; Orb = orbital; Sup = superior; Post = posterior.
** Significant ($p < 0.05$, corrected for along tract comparisons).
*** Significant ($p < 0.05$, corrected for between and along tract comparisons).

determining whether these structural differences may reflect changes in brain structure from prolonged malnutrition, from altered neurodevelopment, or reflect structural differences characteristic to the neuropathology of AN.

We did not observe evidence for decreased FA in AN as compared to the control sample in either left or right tracts of the inferior fronto-occipital fasciculus or cingulate pathways, as had been seen in other studies. The lack of significant FA differences within these pathways and other tracts may be explained by limitations of diffusion-based methods for identifying group differences in FA in small sample sizes or by possible differences between adolescent and adult study populations. Empirical work performed by De Santis and colleagues has estimated that group sizes involving 20 to 30 participants are necessary for observing group FA differences within inferior fronto-occipital fasciculus or cingulate pathways (De Santis et al., 2014). These estimates are comparable to a previous dMRI study of AN in which significant FA differences were observed for these pathways (Frieling et al., 2012). However, a study with a sample only slightly larger than the present study was able to detect evidence for significant group differences in FA of the inferior fronto-occipital fasciculus and cingulate (Kazlouski et al., 2011).

Lack of significant group differences within the cingulate and inferior fronto-occipital fasciculus tracts may also be explained by methodological differences between tractography versus voxel-based studies of AN (Frank et al., 2013; Frieling et al., 2012; Kazlouski et al., 2011). Studies that use whole brain voxel-based methods are susceptible to error based on challenges in the co-registration and normalization process that might result in subtle but significant differences in the composition of voxels in terms of cerebral spinal fluid, gray matter and white matter (Jones and Cercignani, 2010). The methods used in the present study are also vulnerable to similar co-registration errors but do not require normalization of the brain to a common template to identify white matter tracts (Yeatman et al., 2012). In addition, the procedures we used for identifying and segmenting tracts were designed to characterize core tract regions that are anatomically consistent across individuals and therefore less susceptible to partial voluming effects. Alternatively, it is also possible that the present pattern of observations relates to specific clinical characteristics and/or developmental differences of the present adolescent sample in whom myelination of these tracts may not yet be complete.

An unexpected finding was evidence for significantly increased FA in the AN group as compared to the control group within segments of the right anterior thalamic radiation and left anterior superior longitudinal fasciculus. At present, we are unaware of any previous studies of participants with AN that have reported increased FA. However, evidence for increased FA has been reported in other clinical populations where white matter injuries or dysmaturity are predicted, such as children born preterm (Groeschel et al., 2014; Myall et al., 2013). In particular, a recent study by Groeschel et al. (2014) found similar results in a sample of adolescents born preterm. The preterm group had significantly increased FA within crossing fiber regions of the superior longitudinal fasciculus and premotor projections of the anterior thalamic radiations and significantly decreased FA within single fiber regions of the corpus callosum and corticospinal tracts. Such findings in these two clinical groups suggest that the observed pattern of increased FA within the right anterior thalamic radiation and left anterior superior longitudinal fasciculus in the AN group may reflect increased fiber coherence from a reduction in the number or density of crossing fibers (Jones and Cercignani, 2010). We think that this interpretation for increased FA is more plausible than for a compensatory mechanism to have occurred that would lead to greater axonal density or increased levels of myelination in the AN group. The interpretation for increased FA is corroborated by the observation that R1 in the AN group, while not significant, appeared to be generally decreased relative to the control group within similar regions of the right anterior thalamic radiation and left anterior superior longitudinal fasciculus, respectively. Should the increased FA in the AN group reflect increased myelination, we would have expected to observe increased as opposed to decreased R1 within these two pathways. Further, that R1 levels appear to be reduced within regions of increased FA suggests that the neurobiological factors contributing to increased FA in AN, such as increased fiber coherence from axonal loss, may be related to alterations in myelin content.

4.3. Group differences in R1

Consistent with our initial predictions, measures for R1 also demonstrated significant decreases in the AN as compared to the control group within cerebral white matter tracts previously found to have altered white matter microstructure during adulthood and adolescence (Frank et al., 2013; Frieling et al., 2012; Kazlouski et al., 2011). In addition to these pathways, we observed evidence for significantly decreased R1 in bilateral segments of the arcuate fasciculus and medial and posterior subdivisions of the corpus callosum. Evidence for decreased R1 in individuals with AN is consistent with findings that have also observed decreased R1 in other clinical conditions associated white matter injuries, such as multiple sclerosis (Mezer et al., 2013; Mottershead et al., 2003). Future studies employing R1 mapping techniques should include larger samples to replicate these findings and establish whether patterns for wide-spread reductions in R1 are characteristic of white tissue properties changes in AN.

In general, we observed that R1 as a measure was highly sensitive to differences in the microstructural tissue properties in individuals with AN. Tract R1 profiles revealed a consistent pattern for significantly decreased R1 in the AN as compared to the control group in approximately half of all bilateral cerebral white matter tracts and subdivisions of the corpus callosum examined in the present study. Group differences in FA occurred in a smaller subset of white matter tracts. This pattern of findings is generally consistent with empirical evidence demonstrating that larger sample sizes may be required for observing significant group differences with FA than with quantitative T1 ($R1 = 1/T1$) measures (De Santis et al., 2014). In the same study, De Santis et al. (2014) also found that FA, T1, and a separate measure of myelin water fraction (MWF), were most strongly correlated in tract regions comprised of single fiber populations but were not correlated in regions comprised of multiple fiber populations. Such findings provide further evidence that interpretations for FA are likely to be ambiguous within regions of crossing fibers (Jones and Cercignani, 2010) and suggest that FA is mostly likely to only reflect changes in myelin status within regions with a single fiber orientation. Whereas a large majority of cerebral white matter voxels are found to contain multiple fiber crossings, the corpus callosum has been shown to contain mostly fibers of a single orientation (Jeurissen et al., 2013). Taken together, these finding may thus explain why group differences in R1 and FA did not appear to overlap in the cortical tracts examined, but did co-localize within motor subdivisions of the corpus callosum. Finally, it is important to note that while we observed fewer significant group differences using measures for FA than R1, we were nevertheless able to capture significant group differences in FA that were not identified using R1 measures. Such findings indicate that assessing white matter changes associated with specific clinical conditions is likely to be improved by employing multiple indices for white matter microstructure.

4.4. Neurobiology of white matter differences in AN

Taken together, the present pattern of findings suggests that AN is associated with wide-spread white matter changes in cerebral and corpus callosum white matter tracts during adolescence. Based on evidence demonstrating the strong relationship between R1 and variations in myelin content (Stuber et al., 2014), we suspect that decreased R1 in combination with both decreased and increased FA an in the AN group is likely to reflect changes in white matter microstructure related to reduction in myelin content. These findings suggest that weight loss

and starvation may lead to reduced lipid content in the brain. Alternatively, reductions in myelin content could also reflect decreased myelin formation caused by AN disrupting the normal neurodevelopmental process of myelination during adolescence and early adulthood. Decreased R1 could also reflect increases in water content from axonal loss (Paus, 2010) or decreased concentrations of non-heme iron (Stuber et al., 2014). However, it is unlikely that both increased water content and iron loss would occur entirely independent from demyelination (Connor and Menzies, 1996). In-depth understanding of the etiology of white matter disturbances in AN is likely to require further neuroimaging research and studies involving non-human animals models of eating disorders.

The locations of group differences in this study are important for understanding the neuropathological impacts of AN. Interestingly, some of the most significant R1 reductions in the AN group were apparent within white matter tracts known to have large axonal diameters: the corticospinal tracts and subdivisions of the corpus callosum that most closely correspond to the body (motor, temporal, posterior parietal) and splenium (occipital). Some of largest axons in the human brain are found within the internal capsule, which contains fibers belonging to the corticospinal tracts (Lassek, 1942). Axonal diameters are also known to vary among cross-sections of the corpus callosum, with larger axons being most prevalent in medial and posterior cross-sections of the corpus callosum (Aboitiz et al., 1992; Barazany et al., 2009). The tendency for larger diameter axons to have thicker myelin sheaths and therefore higher concentrations of lipids (Paus, 2010) may predispose fibers of the corticospinal tract and corpus callosum to greater degrees of myelin loss that may occur secondary to lipolytic mechanisms from malnutrition (Swayze et al., 2003). Alternatively the present pattern of findings may correspond to developmental patterns observed for myelination. In this scenario, corticospinal tracts, callosal fibers and also posterior pathways such as the inferior fronto-occipital fasciculus may be more susceptible to alterations in myelin content in AN because these pathways are likely to contain greater concentrations of myelin than fiber pathways of the frontal and temporal lobes that are not yet fully myelinated by adolescence (Yakovlev and Lecours, 1967). A third possibility may be that decreased R1 observed within corticospinal and motor pathways of the corpus callosum may reflect injury related to hyperactivity and compulsive exercise behaviors often associated with AN (Davis et al., 1995; Hebebrand et al., 2003). We recognize that the data we collected are correlational and therefore cannot establish whether decreased R1 reflects pre-existing differences in the myelin content of individuals with AN or alterations in myelin content that occur either directly from or secondary to biophysical processes impacted by poor nutrition in AN. Longitudinal studies involving adolescents and adults with AN of different durations will be important for understanding how developmental processes underlying white matter maturation interact with the pathophysiology of AN during adolescence and whether the changes are reversible with weight restoration.

4.5. Association with clinical variables

In the present study, we did not observe significant associations between FA or R1 from areas demonstrating significant group differences and clinical variables of BMI and a composite measure from the EDE-Q. We attribute the lack of significant associations primarily to the modest sample size and restricted range of individual variability in BMI measures and EDE-Q scores. However, a previous study of comparable size reported significant associations between BMI and FA measured from a region in white matter of the left cerebellum (Nagahara et al., 2014). Interestingly, that study did not observe significant group differences between the AN group and normal weight control group in any cerebral white matter region. Future studies employing tractography methods for segmenting cerebellar white matter tracts (Leitner et al., 2015) will be important for establishing whether individual variations in cerebellar white matter microstructure may be associated with BMI in adolescents with AN.

It is also possible that BMI and measures for eating behaviors indexed by the EDE-Q may capture other factors unlikely to account for individual differences contributing to microstructural changes indexed by either FA or R1. For example, reductions in FA and/or R1 that may reflect reductions in myelin from lipolysis may occur independent of factors contributing to individual variations in muscle and bone tissue mass also captured by BMI. Similarly, individual differences in eating behaviors and perceptions about body shape and weight indexed by the EDE-Q may capture variations in psychological traits (e.g., depression or anxiety) that may not be directly related to neuropathological mechanisms underlying microstructural changes observed in AN. Understanding the functional consequences of white matter changes observed in AN will likely require the inclusion of large sample sizes and the collection of specific clinical and behavioral measures that may be more directly related to neurophysiological mechanisms underlying white matter changes in AN.

4.6. Limitations and future directions

The present sample size was modest. However, power calculations performed by De Santis and colleagues have estimated that significant group differences in white matter tracts can be observed with quantitative T1 ($R1 = 1/T1$) measures for sample sizes as small as ~5–6 individuals per group and with FA measures for sample sizes of ~15–30 per group (De Santis et al., 2014). Replication studies with larger sample sizes will be important for establishing the generalizability of the present findings. Given our interest in establishing whether these imaging methods could detect differences in adolescents with AN and controls, we did not acquire an extensive battery of clinical and behavioral measures on either group. Longitudinal follow-up studies will be important to determine whether the identified changes are reversible with weight restoration and correction of the underlying malnutrition.

The present changes observed in white matter microstructure may reflect variations in illness duration of the current AN sample. Longitudinal studies in which neuroimaging scans are acquired closer to initial diagnosis will likely be required to address this issue. Such studies will be helpful for determining which white matter differences may be inherent to AN neuropathology and which differences are responsive to specific medical and psychological interventions. In addition, future neuroimaging studies and research involving animal models for eating disorders should explore whether the pattern for white matter susceptibility may correspond to neurobiological factors related to axonal size, developmental patterns of myelination, and/or injury related to hyperactivity and excessive exercise.

4.7. Conclusions

In conclusion, our study assessed white matter properties in adolescents with AN using advanced techniques for combining dMRI and R1 mapping procedures to examine white matter properties in AN. Our results suggest that there are pervasive changes in white matter microstructure during adolescence that are most likely related to changes in myelin content. In general, the present findings underscore the importance for employing multiple neuroimaging modalities for assessing white matter microstructure changes associated with specific neurological and clinical conditions. Overall, the present findings have important implications for understanding the neurobiological bases for white matter changes observed in AN and invite future research for investigating associations between white matter properties and specific physiological, cognitive, social, or emotional functions affected in AN.

Acknowledgments

We would like to thank the adolescents and families who participated in our study.

Funding

This work has been supported in part by the Mary Gallo Research Fund (NG), and National Institutes of Health, NICHD grants (RO1-HD69162) (HFM). KET is supported by Young Investigator funding provided by the Society for Developmental and Behavioral Pediatrics.

References

Aboitiz, F., Scheibel, A.B., Fisher, R.S., Zaidel, E., 1992. Fiber composition of the human corpus callosum. Brain Res. 598, 143–153.
American Psychiatric Association, 2000. Diagnostic and Statistical Manual of Mental Disorders: DSM-IV. APA, Washington, D.C.
American Psychiatric Association, 2013. Diagnostic and Statistical Manual of Mental Disorders: DSM-5. 5th ed. American Psychiatric Association, Arlington.
Arcelus, J., Mitchell, A.J., Wales, J., Nielsen, S., 2011. Mortality rates in patients with anorexia nervosa and other eating disorders. A meta-analysis of 36 studies. Arch. Gen. Psychiatry 68 (7), 724–731.
Avants, B., Gee, J.C., 2004. Geodesic estimation for large deformation anatomical shape averaging and interpolation. Neuroimage 23 (Suppl. 1), S139–S150.
Barazany, D., Basser, P.J., Assaf, Y., 2009. In vivo measurement of axon diameter distribution in the corpus callosum of rat brain. Brain 132 (Pt 5), 1210–1220.
Basser, P.J., Jones, D.K., 2002. Diffusion-tensor MRI: theory, experimental design and data analysis — a technical review. NMR Biomed. 15 (7–8), 456–467.
Basser, P.J., Pierpaoli, C., 1996. Microstructural and physiological features of tissues elucidated by quantitative-diffusion-tensor MRI. J. Magn. Reson. B 111 (3), 209–219.
Beaulieu, C., 2002. The basis of anisotropic water diffusion in the nervous system — a technical review. NMR Biomed. 15 (7–8), 435–455.
Boghi, A., Sterpone, S., Sales, S., D'Agata, F., Bradac, G.B., Zullo, G., et al., 2011. In vivo evidence of global and focal brain alterations in anorexia nervosa. Psychiatry Res. Neuroimaging 192, 154–159.
Bottomley, P.A., Foster, T.H., Argersinger, R.E., Pfeifer, L.M., 1984. A review of normal tissue hydrogen NMR relaxation times and relaxation mechanisms from 1–100 MHz: dependence on tissue type, NMR frequency, temperature, species, excision, and age. Med. Phys. 11, 425–448.
Castro-Fornieles, J., Bargallo, N., Lazaro, L., Andres, S., Falcon, C., Plana, M.T., et al., 2009. A cross-sectional and follow-up voxel-based morphometric MRI study in adolescent anorexia nervosa. J. Psychiatr. Res. 43 (3), 331–340.
Catani, M., Allin, M.P.G., Husain, M., Pugliese, L., Mesulam, M.M., Murrary, R.M., et al., 2007. Symmetries in human brain language pathways correlated with verbal recall. PNAS 104 (43), 17163–17168.
Chang, L.C., Jones, D.K., Pierpaoli, C., 2005. RESTORE: robust estimation of tensors by outlier rejection. Magn. Reson. Med. 53 (5), 1088–1095.
Connor, J.R., Menzies, S.L., 1996. Relationship of iron to oligodendrocytes and myelination. Glia 17, 83–93.
Davis, C., Kennedy, S.H., Ralevski, E., Dionne, M., Brewer, H., Neitzer, C., et al., 1995. Obsessive compulsiveness and physical activity in anorexia nervosa and high-level exercising. J. Psychosom. Res. 39, 967–976.
De Santis, S., Drakesmith, M., Bells, S., Assaf, Y., Jones, D.K., 2014. Why diffusion tensor MRI does well only some of the time: variance and covariance of white matter tissue microstructure attributes in the living human brain. Neuroimage 89, 35–44.
Feldman, H.M., Yeatman, J.D., Lee, E.S., Barde, L.H., Gaman-Bean, S., 2010. Diffusion tensor imaging: a review for pediatric researchers and clinicians. J. Dev. Behav. Pediatr. 31 (4), 346–356.
Fram, E.K., Herfkens, R.J., Johnson, G.A., Glover, G.H., Karis, J.P., Shimakawa, A., et al., 1987. Rapid calculation of T1 using variable flip angle gradient refocused imaging. Magn. Reson. Imaging 5, 201–208.
Frank, G.K., Shott, M.E., Hagman, J.O., Yang, T.T., 2013. Localized brain volume and white matter integrity alterations in adolescent anorexia nervosa. J. Am. Acad. Child Adolesc. Psychiatry 52 (10), 1066–1075 (e5).
Frieling, H., Fischer, J., Wilhelm, J., Engelhorn, T., Bleich, S., Hillemacher, T., et al., 2012. Microstructural abnormalities of the posterior thalamic radiation and the mediodorsal thalamic nuclei in females with anorexia nervosa—a voxel based diffusion tensor imaging (DTI) study. J. Psychiatr. Res. 46 (9), 1237–1242.
Giedd, J.N., 2008. The teen brain: insights from neuroimaging. J. Adolesc. Health 42, 335–343.
Golden, N.H., Ashtari, M., Kohn, M.R., Patel, M., Jacobson, M.S., Fletcher, A., et al., 1996. Reversibility of cerebral ventricular enlargement in anorexia nervosa, demonstrated by quantitative magnetic resonance imaging. J. Pediatr. 128 (2), 296–301.
Groeschel, S., Tournier, J.D., Northam, G.B., Baldeweg, T., Wyatt, J., Vollmer, B., et al., 2014. Identification and interpretation of microstructural abnormalities in motor pathways in adolescents born preterm. Neuroimage 87, 209–219.
Hebebrand, J., Exner, C., Hebebrand, K., Holtkamp, C., Casper, R.C., Remschmidt, H., et al., 2003. Hyperactivity in patients with anorexia nervosa and in semistarved rats: evidence for a pivotal role of hypoleptinemia. Physiol. Behav. 79 (1), 25–37.
Hoffman Jr., G.W., Ellinwood Jr., E.H., Rockwell, W.J., Herfkens, R.J., Nishita, J.K., Guthrie, L.F., 1989. Cerebral atrophy in anorexia nervosa: a pilot study. Biol. Psychiatry 26 (3), 321–324.
Hua, K., Zhang, J., Wakana, S., Jiang, H., Li, X., Reich, D.S., et al., 2008. Tract probability maps in stereotaxic spaces: analyses of white matter anatomy and tract-specific quantification. Neuroimage 39 (1), 336–347.
Jeurissen, B., Leemans, A., Tournier, J.D., Jones, D.K., Sijbers, J., 2013. Investigating the prevalence of complex fiber configurations in white matter tissue with diffusion magnetic resonance imaging. Hum. Brain Mapp. 34 (2747–2766).
Jones, D.K., Cercignani, M., 2010. Twenty-five pitfalls in the analysis of diffusion MRI data. NMR Biomed. 23 (7), 803–820.
Katzman, D.K., Lambe, E.K., Mikulis, D.J., Ridgley, J.N., Goldbloom, D.S., Zipursky, R.B., 1996. Cerebral gray matter and white matter volume deficits in adolescent girls with anorexia nervosa. J. Pediatr. 129 (6), 794–803.
Katzman, D.K., Zipursky, R.B., Lambe, E.K., Mikulis, D.J., 1997. A longitudinal magnetic resonance imaging study of brain changes in adolescents with anorexia nervosa. Arch. Pediatr. Adolesc. Med. 151 (8), 793–797.
Kazlouski, D., Rollin, M.D., Tregellas, J., Shott, M.E., Jappe, L.M., Hagman, J.O., et al., 2011. Altered fimbria-fornix white matter integrity in anorexia nervosa predicts harm avoidance. Psychiatry Res. 192 (2), 109–116.
Kingston, K., Szmukler, G., Andrewes, D., Tress, B., Desmond, P., 1996. Neuropsychological and structural brain changes in anorexia nervosa before and after refeeding. Psychol. Med. 26 (1), 15–28.
Kucharczyk, W., Macdonald, P.M., Stanisz, G.J., Henkelman, R.M., 1994. Relaxivity and magnetization transfer of white matter lipids at MR imaging Importance of cerebrosides and pH. Radiology 192, 521–529.
Lassek, A.M., 1942. The human pyramidal tract V. Postnatal changes in the axons of the pyramids. Arch. Neurol. Psychiatr. 47, 422–427.
Lebel, C., Beaulieu, C., 2009. Lateralization of the arcuate fasciculus from childhood to adulthood and its relation to cognitive abilities in children. Hum. Brain Mapp. 30, 3563–3573.
Leitner, Y., Travis, K.E., Ben-Shachar, M., Yeom, K.W., Feldman, H.M., 2015. Tract profiles of the cerebellar white matter pathways in children and adolescents. Cerebellum http://dx.doi.org/10.1007/s12311-015-0652-1 (E-pub ahead of print).
Lutti, A., Hutton, C., Finsterbusch, J., Helms, G., Weiskopf, N., 2010. Optimization and validation of methods for mapping of the radiofrequency transmit field at 3 T. Magn. Reson. Med. 64 (1), 229–238.
Mansfield, P., 1982. NMR Imaging in Biomedicine: Supplement 2, Advances in Magnetic Resonance. Academic, New York.
Mezer, A., Yeatman, J.D., Stikov, N., Kay, K.N., Cho, N.J., Dougherty, R.F., et al., 2013. Quantifying the local tissue volume and composition in individual brains with magnetic resonance imaging. Nat. Med. 19 (12), 1667–1672.
Mishra, A., Anderson, A.W., Wu, X., Gore, J.C., Ding, Z., 2010. An improved Bayesian tensor regularization and sampling algorithm to track neuronal fiber pathways in the language circuit. Med. Phys. 37 (8), 4274.
Mottershead, J.P., Schmierer, K., Clemence, M., Thornton, J.S., Scaravilli, F., Barker, G.J., et al., 2003. High field MRI correlates of myelin content and axonal density in multiple sclerosis—a post-mortem study of the spinal cord. J. Neurol. 250 (11), 1293–1301.
Muhlau, M., Gaser, C., Ilg, R., Conrad, B., Leibl, C., Cebulla, M.H., et al., 2007. Gray matter decrease of the anterior cingulate cortex in anorexia nervosa. Am. J. Psychiatr. 64, 1850–1857.
Myall, N.J., Yeom, K.W., Yeatman, J.D., Gaman-Bean, S., Feldman, H.M., 2013. Case series: fractional anisotropy along the trajectory of selected white matter tracts in adolescents born preterm with ventricular dilation. J. Child Neurol. 28 (6), 774–780.
Nagahara, Y., Nakamae, T., Nishizawa, S., Mizuhara, Y., Moritoki, Y., Wada, Y., et al., 2014. A tract-based spatial statistics study in anorexia nervosa: abnormality in the fornix and the cerebellum. Prog. Neuropsychopharmacol. Biol. Psychiatry 51, 72–77.
Nichols, T.E., Holmes, A.P., 2001. Nonparametric permutation tests for functional neuroimaging: a primer with examples. Hum. Brain Mapp. 15, 1–25.
Paus, T., 2010. Growth of white matter in the adolescent brain: myelin or axon? Brain Cogn. 72 (1), 26–35.
Reese, T.G., Heid, O., Weisskoff, R.M., Wedeen, V.J., 2003. Reduction of eddy-current-induced distortion in diffusion MRI using a twice-refocused spin echo. Magn. Reson. Med. 49 (1), 177–182.
Roberto, C.A., Mayer, L.E., Brickman, A.M., Barnes, A., Muraskin, J., Yeung, L.K., et al., 2011. Brain tissue volume changes following weight gain in adults with anorexia nervosa. Int. J. Eat. Disord. 44 (5), 406–411.
Rohde, G.K., Barnett, A.S., Basser, P.J., Marenco, S., Pierpaoli, C., 2004. Comprehensive approach for correction of motion and distortion in diffusion-weighted MRI. Magn. Reson. Med. 51 (1), 103–114.
Rooney, W.D., Johnson, G., Li, X., Cohen, E.R., Kim, S.G., Ugurbil, K., et al., 2007. Magnetic field and tissue dependencies of human brain longitudinal ^1H_2O relaxation in vivo. Magn. Reson. Med. 57 (2), 308–318.
Sherbondy, A., Akers, D., Mackenzie, R., Dougherty, R., Wandell, B., 2005. Exploring connectivity of the brain's white matter with dynamic queries. IEEE Trans. Vis. Comput. Graph. 11 (4), 419–430.
Stikov, N., Perry, L.M., Mezer, A., Rykhlevskaia, E., Wandell, B.A., Pauly, J.M., et al., 2011. Bound pool fractions complement diffusion measures to describe white matter micro and macrostructure. Neuroimage 54 (2), 1112–1121.
Stuber, C., Morawski, M., Schafer, A., Labadie, C., Wahnert, M., Leuze, C., et al., 2014. Myelin and iron concentration in the human brain: a quantitative study of MRI contrast. Neuroimage 93 (Pt 1), 95–106.
Swayze II, V.W., Andersen, A., Arndt, S., Rajarethinam, R., Fleming, F., Sato, Y., et al., 1996. Reversibility of brain tissue loss in anorexia nervosa assessed with a computerized Talairach 3-D proportional grid. Psychol. Med. 26 (2), 381–390.

Swayze II, V.W., Andersen, A.E., Andreasen, N.C., Arndt, S., Sato, Y., Ziebell, S., 2003. Brain tissue volume segmentation in patients with anorexia nervosa before and after weight normalization. Int. J. Eat. Disord. 33 (1), 33–44.
Tofts, P., 2003. Quantitative MRI of the Brain: Measuring Changes Caused by Disease. Wiley, West Sussex, UK.
Via, E., Zalesky, A., Sanchez, I., Forcano, L., Harrison, B.J., Pujol, J., et al., 2014. Disruption of brain white matter microstructure in women with anorexia nervosa. J. Psychiatry Neurosci. 39 (6), 367–375.
Wakana, S., Jiang, H., Nagae-Poetscher, L.M., van Zijl, P.C., Mori, S., 2004. Fiber tract-based atlas of human white matter anatomy. Radiology 230 (1), 77–87.
Yakovlev, P., Lecours, A., 1967. The Myelogenetic Cycles of Regional Maturation of the Brain. Blackwell, Oxford.
Yarnykh, V.L., 2010. Optimal radiofrequency and gradient spoiling for improved accuracy of T1 and B1 measurements using fast steady-state techniques. Magn. Reson. Med. 63 (6), 1610–1626.
Yau, W.Y., Bischoff-Grethe, A., Theilmann, R.J., Torres, L., Wagner, A., Kaye, W.H., et al., 2013. Alterations in white matter microstructure in women recovered from anorexia nervosa. Int. J. Eat. Disord. 46 (7), 701–708.
Yeatman, J.D., Dougherty, R.F., Rykhlevskaia, E., Sherbondy, A.J., Deutsch, G.K., Wandell, B., et al., 2011. Anatomical properties of the arcuate fasciculus predict phonological and reading skills in children. J. Cogn. Neurosci. 23 (11), 3304–3317.
Yeatman, J.D., Dougherty, R.F., Myall, N.J., Wandell, B.A., Feldman, H.M., 2012. Tract profiles of white matter properties: automating fiber-tract quantification. PLoS One 7 (11), e49790.
Yeatman, J.D., Wandell, B.A., Mezer, A.A., 2014. Lifespan maturation and degeneration of human brain white matter. Nat. Commun. 5, 4932.